School of
ENGINEERING
DUKE UNIVERSITY

DUKE UNIVERSITY

Department of Electrical Engineering
School of Engineering

Final Report
September 1, 1986 - June 30, 1990
Contract No. N00014-86-K-0787

ADAPTIVE ACOUSTIC SIGNAL DETECTION

REPORT DOCUMENTATION PAGE

Form Approved
OMB No 0704-0188

1. AGENCY USE ONLY (Leave blank)	2. REPORT DATE	3. REPORT TYPE AND DATES COVERED
	1990	Final

4. TITLE AND SUBTITLE
Adaptive Acoustic Signal Detection

5. FUNDING NUMBERS
Contract No.
N00014-86-k-0787

6. AUTHOR(S)
L. W. Nolte

7. PERFORMING ORGANIZATION NAME(S) AND ADDRESS(ES)
Duke University
Durham, NC 27707

8. PERFORMING ORGANIZATION REPORT NUMBER

9. SPONSORING/MONITORING AGENCY NAME(S) AND ADDRESS(ES)
Office of Naval Research (Code 1125UA)
800 N. Quincy Street
Arlington, VA

10. SPONSORING/MONITORING AGENCY REPORT NUMBER

11. SUPPLEMENTARY NOTES
A

12a. DISTRIBUTION/AVAILABILITY STATEMENT

12b. DISTRIBUTION CODE

13. ABSTRACT (Maximum 200 words)

In this research, optimum ocean-model-based detection algorithms were developed for signals received through an inhomogeneous acoustic ocean medium. These optimal algorithms are driven by the knowledge of the underlying wavefront propagation in an inhomogeneous ocean medium. Comparison of narrowband and broadband performance as a function of range for both range-independent and range-dependent ocean environments were made. In addition, sensitivity of detection performance to mismatch in the sound speed profile as a function of range and transmitted were obtained. A new a posteriori probability source localization algorithm was developed which exhibits much less sensitivity to the underlying assumptions of the ocean acoustic medium (sound speed profiles) than do the classical matched field algorithms. The design and performance of optimal and fault-tolerant distributed detection networks, from a signal detection theory point of view, were also developed.

14. SUBJECT TERMS	15. NUMBER OF PAGES
Source localization, matched-field processing signal detection	31
	16. PRICE CODE

17. SECURITY CLASSIFICATION OF REPORT	18. SECURITY CLASSIFICATION OF THIS PAGE	19. SECURITY CLASSIFICATION OF ABSTRACT	20. LIMITATION OF ABSTRACT
Unclassified	Unclassified	Unclassified	UL

DUKE UNIVERSITY

Department of Electrical Engineering
School of Engineering

Final Report
September 1, 1986 - June 30, 1990
Contract No. N00014-86-K-0787

ADAPTIVE ACOUSTIC SIGNAL DETECTION

Approved: L. W. Nolte

L. W. Nolte, Principal Investigator

Prepared under: Office of Naval Research (Code 1125UA)
Contract No. N00014-86-K-0787

1 Introduction

The focus of this research was to determine the impact on detection and localization performance of uncertainties in an inhomogeneous ocean acoustic medium, as characterized by the sound speed profile. The framework is the development of signal detection and estimation theory in passive ocean surveillance situations of interest to the U.S. Navy.

In order to determine the maximum attainable signal detection performance, it is important that the signal processing techniques considered be driven by the knowledge of the physics of the underlying acoustic wavefront propagation. The ocean acoustic tomography group has demonstrated that it is possible to remotely measure the sound speed profile. An important issue is to determine optimum ocean surveillance detection performance, not only as a function of transmitted signal and noise characteristics, but as a function of the degree of our knowledge of the ocean acoustic medium, as characterized by the sound speed profile.

2 Approach

The basic approach couples signal detection and estimation theory with the physics of underwater acoustic wavefront propagation in an inhomogeneous long range ocean environment. This approach is applicable for both narrow and wideband acoustic signals. In this approach the knowledge of the sound speed profile is utilized, along with numerical ray tracing techniques, to derive the structure of optimum (likelihood ratio) detection and localization (a posteriori probabilities) algorithms. Signal detection theory also provides a framework for determining the maximum detection performance obtainable in range-depth space, in terms of the ROC (receiver operator characteristic), for various underwater acoustic channel scenarios.

3 Summary of Research Accomplished

Results have been obtained in:

- Development of optimum ocean-model-based detection algorithms [Lazoff]. Effects of signal bandwidth on detection performance of optimal ocean-model-based algorithms, for signals received through an inhomogeneous acoustic ocean medium. These optimal algorithms are driven by the knowledge of the underlying wavefront propagation in an inhomogeneous ocean medium. Comparison of narrowband and broadband performance as a function of range for both range-independent and range-dependent (GDEM database) ocean environments. Sensitivity of detection performance to mismatch in the sound speed profile as a function of range and transmitted signal bandwidth.

- Performance of wideband matched-field localization algorithms [Clarke, Rausch]. Sensitivity of matched-field localization to the sound speed profile information.
- Development of new a posteriori probability source localization algorithms [Richardson, Nolte]. These algorithms exhibit much less sensitivity to the underlying assumptions of the ocean acoustic medium (sound speed profiles) than do the classical matched field algorithms.
- Multi-site signal detection [Reibman, Nolte]. Design and performance of optimal and fault-tolerant distributed detection networks. These results are applicable to the multi-site, widely-spaced arrays situation in passive ocean surveillance. These research results were obtained primarily in a previous research period but many of the published papers were completed during this period.

3.1 Optimal Detection Performance and Sensitivity in an Inhomogeneous Ocean Acoustic Medium, Wideband versus Narrowband Signals

3.1.1 Introduction

In this work the optimum detectability of a signal received through an inhomogeneous acoustic ocean medium was obtained as a function of the bandwidth of the signal [Lazoff]. The ocean medium was characterized by two situations; a range-independent set of sound speed profiles, and a range-dependent set taken from the GDEM database across the Gulf Stream. Optimum signal detection theory (likelihood ratio) was used to derive the optimum detector driven by the physics of the ocean acoustic medium. In addition, the sensitivity of detection performance to mismatch in the sound speed profile was obtained as a function of the bandwidth of the signal.

The ocean was modelled as a time-invariant but spatially-varying transfer function for a large grid of received points. At the i^{th} received point, the transfer function is given by

$$H_i(f) = \sum_p c_{ip} e^{-j\omega\tau_{ip}} \tag{1}$$

In this equation p is the path index, f is the transmitted frequency $\omega = 2\pi f$, c_{ip} is the amplitude and τ_{ip} is the propagation time of the p^{th} path at the i^{th} received point. The model parameters depend upon the source location and the received point. The corresponding channel impulse response is

$$h_i(t) = \sum_p c_{ip}\delta(t - \tau_{ip}) \tag{2}$$

where $\delta(t)$ is the impulse function.

The sound speed profile used is labelled "orig" in Figure 1. Profiles labelled 1,2,3 and 4 in Figure 1 are used for the sensitivity studies of sound speed profile mismatch. Profile 1 is the furthest from the original, continuing until Profile 4 is the closest to the original. The original profile has a surface velocity of 1542 meters/sec, and a sound axis velocity of 1489 m/s at an axis depth of 1200 meters. Profile 4 only differs in its surface velocity by 1 m/s, while Profile 1 differs by 14 m/s. Also the sound speed axis for Profile 1 is at a depth of 1000 meters, and the velocity at the axis is 1486 m/s. The major differences are above the sound speed axis.

3.1.2 Narrowband Signals

Here the transmitted signal is modelled as a narrowband signal

$$s(t) = A\cos(\omega t + \Phi) \tag{3}$$

where A is the amplitude of the signal, ω is the radian frequency, and Φ is the phase. Specific results were obtained for a low frequency signal of 40 Hz.

The detectability index (which characterizes the ROC) for the optimum detector is proportional to the square of the received signal amplitude

$$d_M \propto a^2 \tag{4}$$

when the assumed sound speed profile of the detector is matched to the actual sound speed profile. However, for the sound speed profile mismatched case the detectability index is proportional to the square of the received amplitude times the square of the cosine of the difference in phase between the expected wavefront and the actual wavefront.

$$d_{MM} \propto a^2\cos^2(\phi - \phi_0) \tag{5}$$

a is the signal amplitude received using the actual sound velocity profile, ϕ is the phase of the received signal using the actual sound speed profile, and ϕ_0 is the phase of the signal that would be received using the assumed sound velocity profile.

A plot of the detectability index for the matched case for the original profile is shown in Figure 2 for a range of 17,760 to 35,520 meters. White corresponds to a high detectability index; black corresponds to a poor detectability index.

In Figure 3 is shown a plot of the detectability index had the processor assumed Profile-4, although the actual profile is "orig". These two profiles differ only by about 1 m/s at the surface. As range increases, an increasing area of poor detectability appears due to the very small mismatch in the sound speed profiles.

For long range detection, the loss in detection performance can become significant for a narrowband signal as a function of mismatch of the sound speed profile.

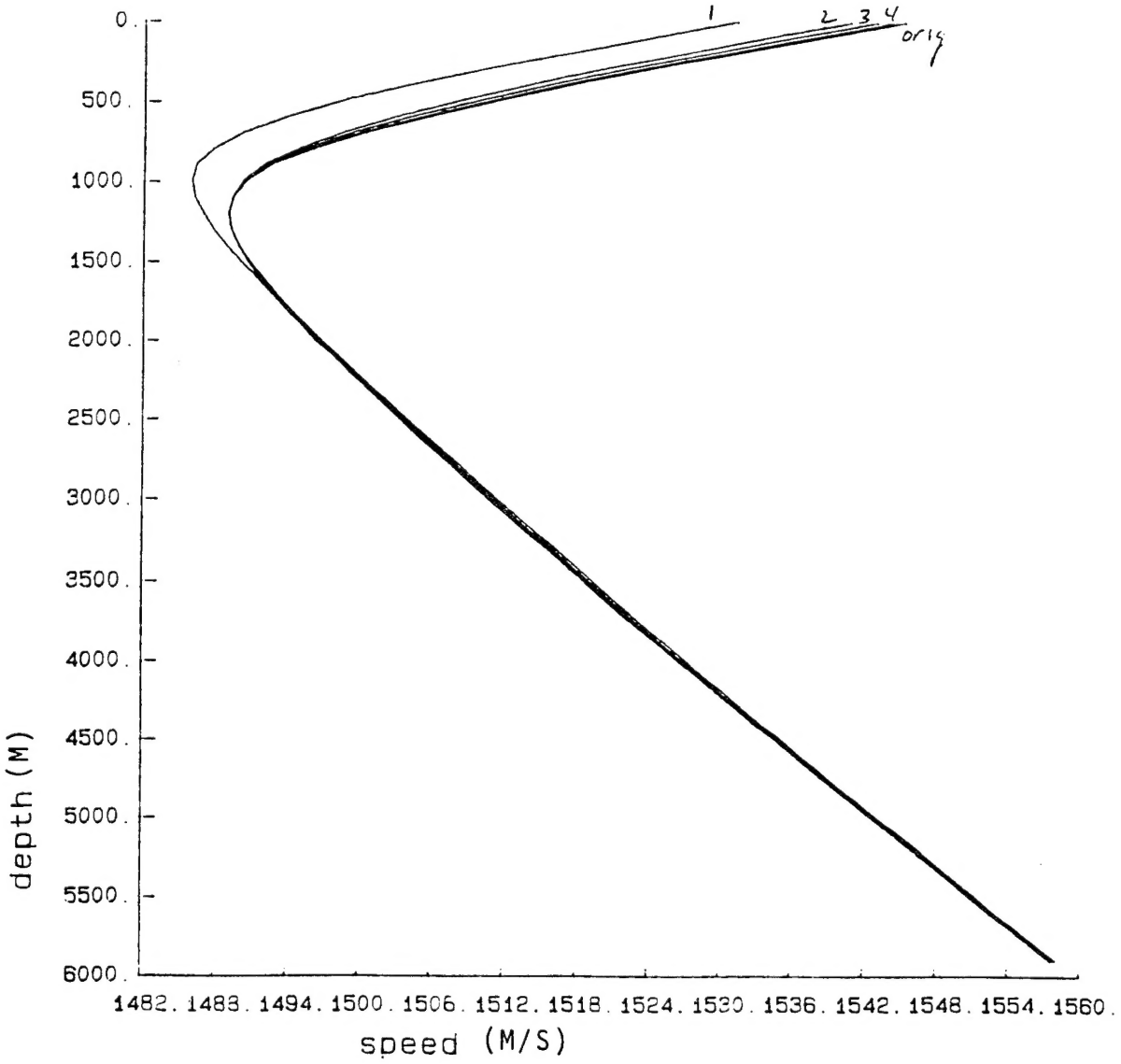

Figure 1: Sound velocity profiles.

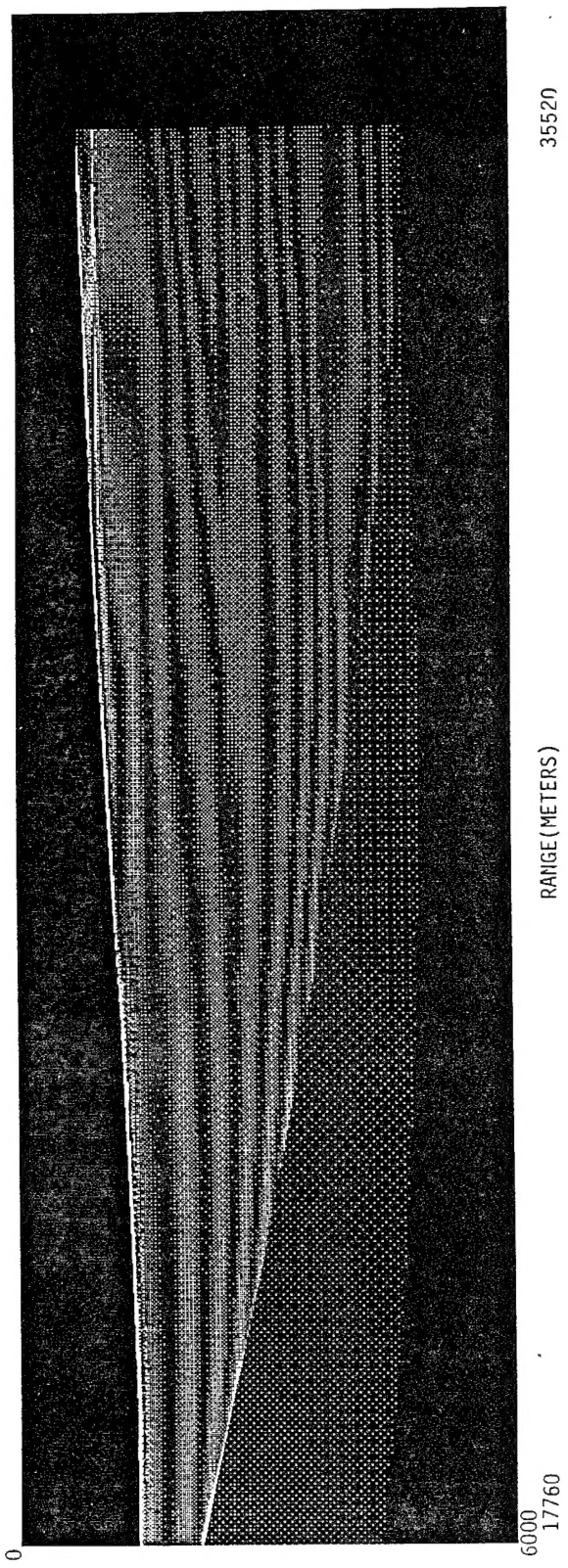

Figure 2: Detectability index for original profile: 17,760 - 35,520 m.

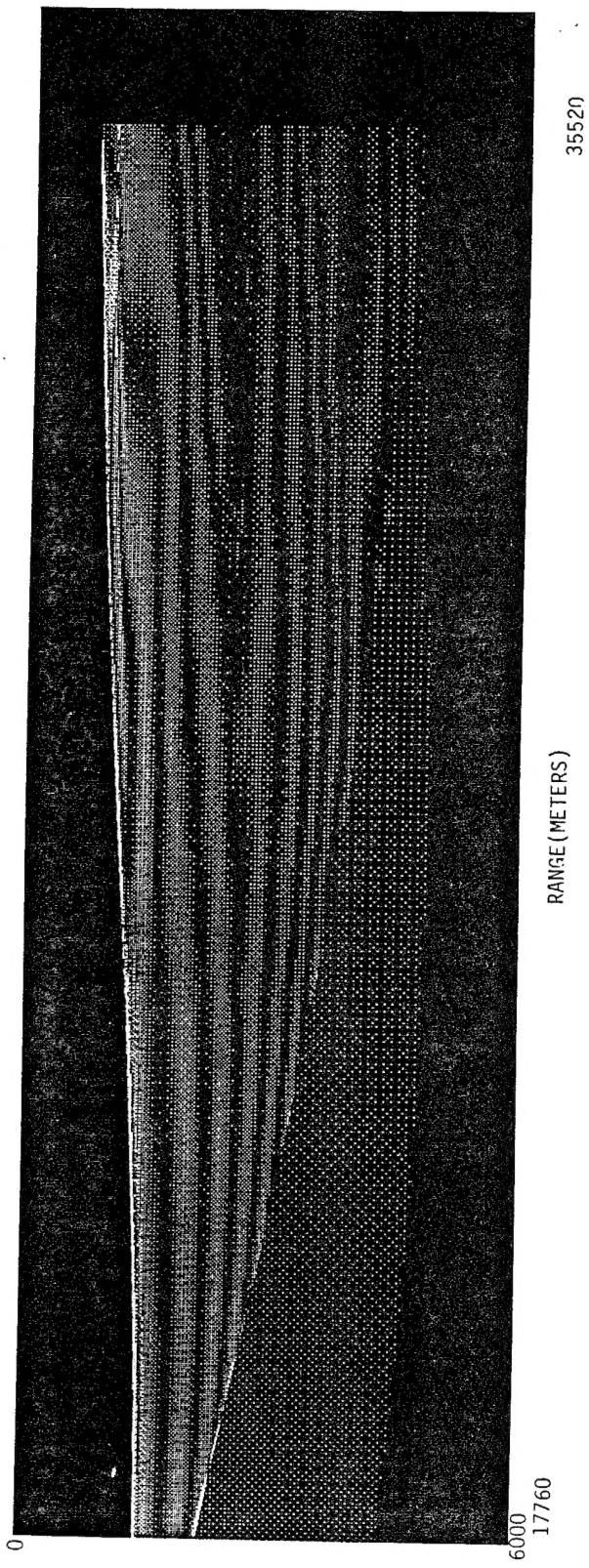

Figure 3: Detectability index for Profile 4: 17,760 - 35,520 m.

3.1.3 Wideband Signals

For an ideal wideband signal, $s(t)$,

$$|S(f)|^2 = E_s, \ -\infty < f < \infty \tag{6}$$

where $S(f)$ is the Fourier Transform of the signal $s(t)$, f is the frequency. and E_s is a constant. The detectability index, in the frequency domain, is given by

$$d_{WM} \propto \int_{-\infty}^{\infty} |S(f)|^2 \, |H_D(f)|^2 \, df \tag{7}$$

$H_D(f)$ is the ocean transfer function for which the processor was designed which is defined as

$$H_D(f) = \sum_p c_p e^{-j\omega\tau_p} \tag{8}$$

p is the path index, c is the path amplitude, $\omega = 2\pi f$, and τ_p is the path delay. Substituting into Equation 7, the wideband matched detectability index is obtained.

$$d_{WM} \propto \sum_p c_p^2 \tag{9}$$

For the 17,760 - 35,520 range, the wideband detectability index for the original profile is plotted in Figure 4. This plot is much improved over the corresponding narrowband matched case. Many of the interference patterns have been smoothed out.

3.1.4 Wideband Approximation

Matched Case In this section we consider what practical bandwidth would be needed to approximate the wideband signal results of the previous section. A Gaussian signal was used, with the variance being the parameter that determines the bandwidth. This signal is

$$s(t) = \frac{A}{T} e^{-\frac{1}{2T^2}(t-t_d)^2} \cos[\omega_o(t - t_d)] \tag{10}$$

A is just a scaling factor, T is the variance, t_d is the time delay for when the signal was transmitted, and ω_o is the center frequency in radians. The effective bandwidth, W, of this signal is

$$W = \frac{1}{2\pi T}\sqrt{\ln 2} \tag{11}$$

The detectability index, using Equation 7, for the Gaussian signal $s(t)$ is

$$d_M \propto \sum_p \sum_{p'} c_p c_{p'} e^{-\frac{(\tau_{p'}-\tau_p)^2}{4T^2}} \left[\cos[\omega_o(\tau_{p'} - \tau_p)] + e^{-T^2\omega_o^2}\right] \tag{12}$$

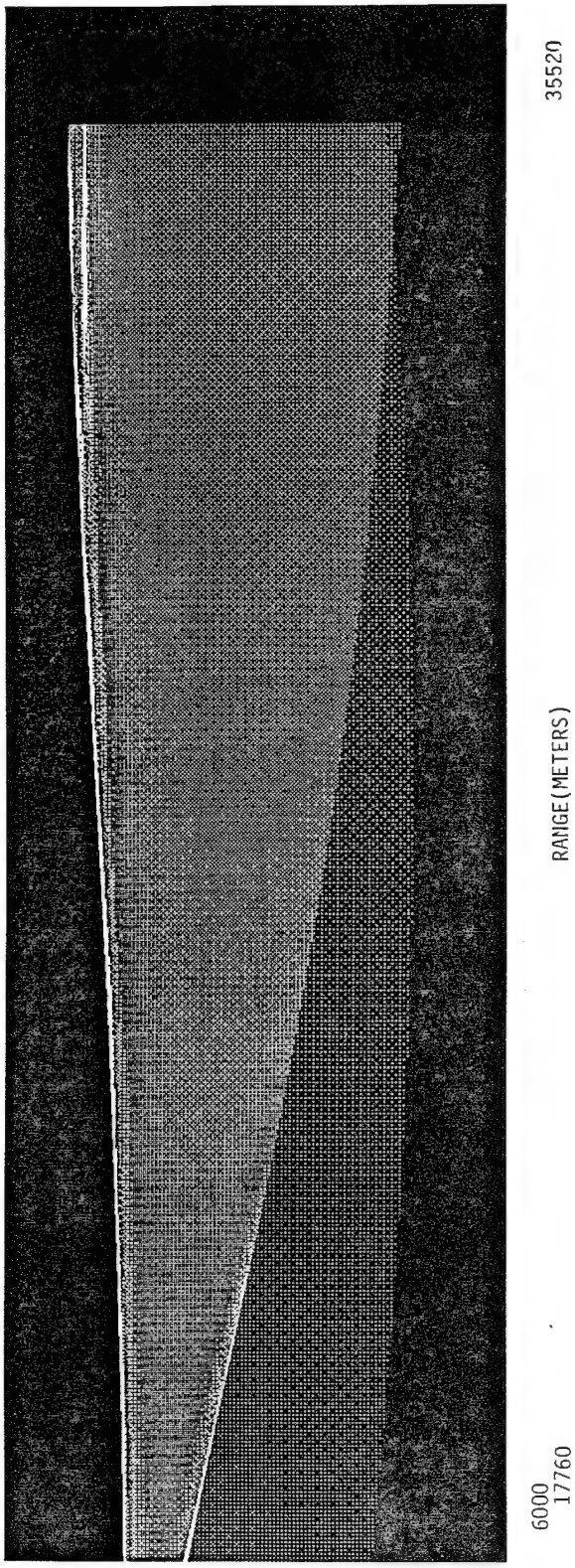

Figure 4: Wideband detectability index for profile 0: 17,760 - 35,520 m.

This can be rearranged and put in the form

$$d_M \propto \sum_p c_p^2 + \frac{1}{1+e^{-T^2\omega_o^2}} \sum_p \sum_{p' \neq p} c_p c_{p'} e^{-\frac{(\tau_{p'}-\tau_p)^2}{4T^2}} \left[\cos[\omega_o(\tau_{p'}-\tau_p)] + e^{-T^2\omega_o^2}\right] \tag{13}$$

As $T \to 0$, $W \to \infty$, and the exponential $e^{-\frac{(\tau_{p'}-\tau_p)^2}{4T^2}} \to 0$ and we approach the detectability index of the wideband case. If the exponential term above has a value less than e^{-4}, the interference term has a magnitude that is approximately 2% of the wideband term. This will occur if the following condition is satisfied.

$$T < \frac{|\tau_{p'} - \tau_p|}{4} \quad \forall p, p' \tag{14}$$

The bandwidth depends upon the time differences of the path delays. Using this value of T and solving for W, the signal bandwidth must satisfy the following.

$$W > \frac{2}{\pi |\tau_{p'} - \tau_p|} \sqrt{\ln 2} \quad \forall p, p' \tag{15}$$

A bandwidth calculation at a range of 48,000 meters and 2400 meters in depth gives a bandwidth of $W > 3.31$ Hz. Performance was obtained as a function of signal bandwidth to determine what bandwidth approximated wideband in terms of the detectability index. Performance was plotted as a function of bandwidth and range. To average over depth, acceptable performance was actually plotted. This is the percentage of points over depth in which the finite bandwidth detectability index has no more than a 3 dB drop over the wideband detectability index. Transmitting a 40 Hz signal, the plot in Figure 5 is obtained. Range increases from left to right, and the bandwidth W increases from front to back. The percentage of points with acceptable performance is plotted on the vertical axis.

As is expected, the performance gets better as the bandwidth is increased. The curve at the front of the plot corresponds to the narrowband case, or $W = 0$. A rapid improvement occurs for the first 1 or 2 Hz, and then the performance levels off. A 1 to 2 Hz bandwidth signal is a good approximation to wideband, with little improvement occurring for wider bandwidths.

Mismatched Case - Wideband The detectability index in the mismatched case is given by

$$d_{MM} \propto \frac{\left[\int_{-\infty}^{\infty} |S(f)|^2 H_D^*(f) H_T(f) df\right]^2}{\int_{-\infty}^{\infty} |S(f)|^2 |H_D(f)|^2 df} \tag{16}$$

As in the matched case, $S(f)$ is the Fourier Transform of the Gaussian input signal $s(t)$, and $H_D(f)$ is the ocean transfer function for which the processor is designed. $H_T(f)$ is the true ocean transfer function, and is calculated from the actual sound velocity profile.

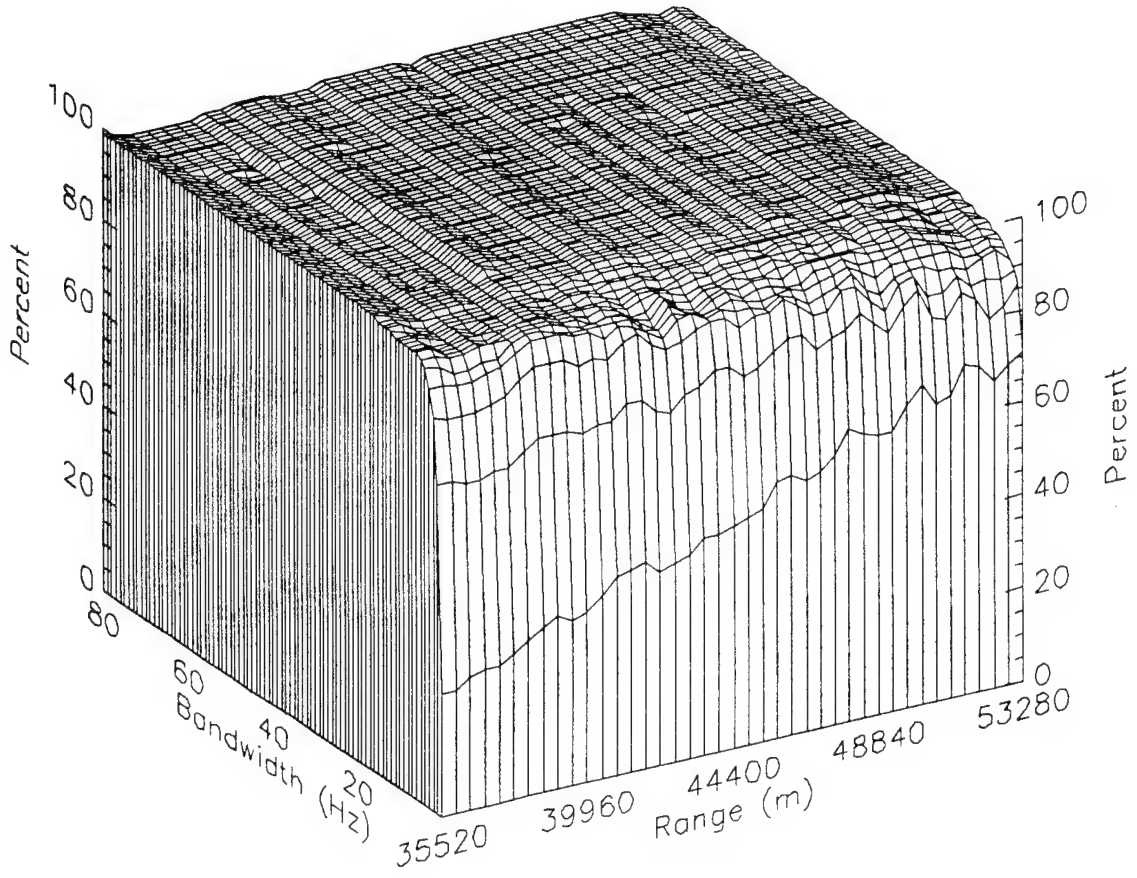

Figure 5: Percentage of points with acceptable performance: f = 40 Hz.

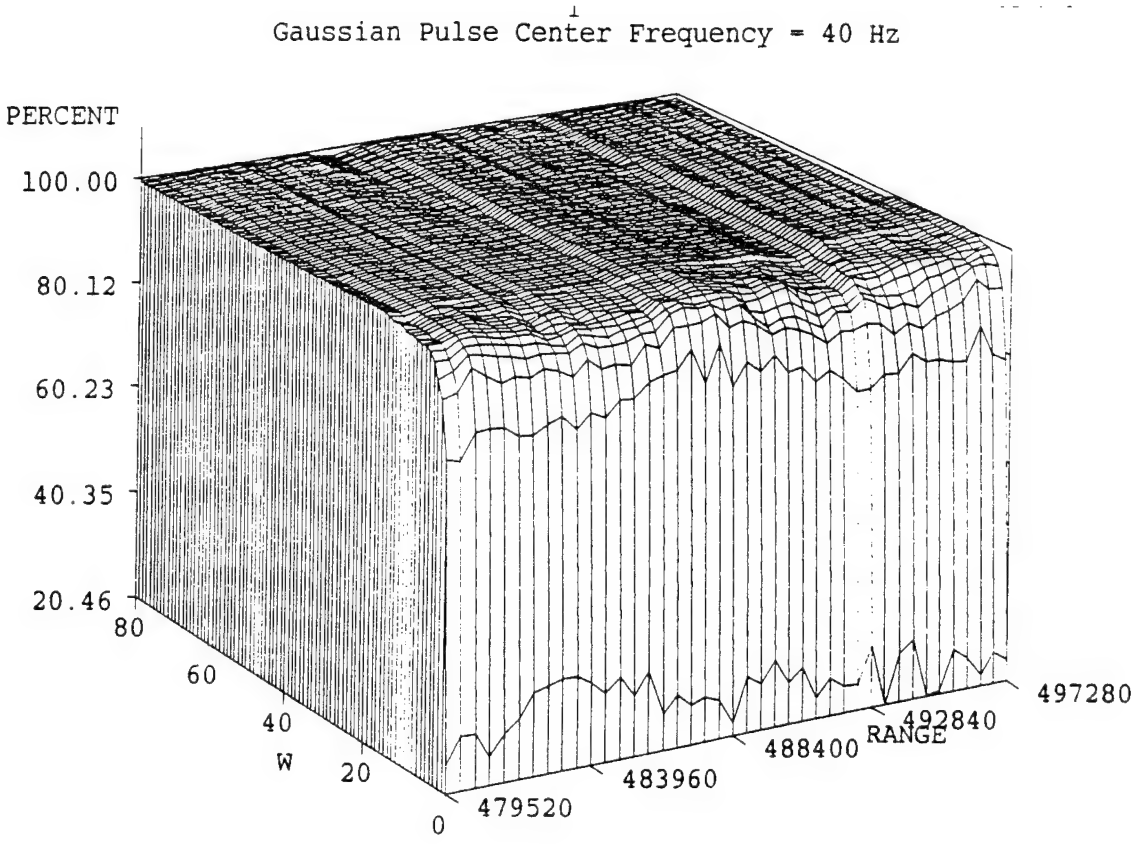

Figure 6: Percentage of points with acceptable performance: f = 40 Hz.

It has the same form as the designed transfer function, except that the values of the delays and the amplitudes will be different.

$$H_T(f) = \sum_m a_m e^{-j\omega_o t_m} \tag{17}$$

For the 35,520 - 53,280 meter range, a three dimensional plot is produced having the same appearance as in the matched case. Figure 7 is for a carrier frequency of 40 Hz. The performance decreases with range, and even a 1 or 2 Hz bandwidth will not produce good results. Larger bandwidths are preferred if exact knowledge of the ocean is available. However, smaller bandwidths are preferred in the mismatched case. The range at which the signal can be detected is limited by the amount of mismatch in the sound velocity profiles.

3.1.5 Range Dependent Ocean

The Generalized Digital Environmental Model (GDEM) database was used as a source of range-dependent sound speed profiles. A rapidly changing section of the ocean was used. In particular, signal transmission was attempted through the gulf stream off the eastern coast of Florida. The gulf stream provides a set of sound velocity profiles that can differ greatly over a short distance. This can be seen by examining the plot in Figure 8. These differences can be more easily seen if the gradient between adjacent profiles is plotted as is done in Figure 9. It is seen that most of the changes occur near the sound speed axis, and also in the near range of transmission. After 300 km or so, the gulf stream ends.

A similar analysis was performed using a range dependent ray tracing algorithm. The first scenario was the case where a 40 Hz signal was transmitted over a distance of 35,520 to 53,280 meters. Performance is plotted in Figure 10. It appears that a wider bandwidth is needed in the range dependent case.

3.2 Wideband Source Localization in an Inhomogeneous Ocean Acoustic Medium

Wideband localization performance was investigated using both matched field processing and a posteriori probability algorithms[Clarke, Rausch]. In addition, the sensitivity of matched field localization to the assumed knowledge of the sound speed profile was investigated.

The matched field approach used a two-dimensional correlation of the received time wavefront with an ensemble of replica wavefronts obtained from a ray tracing acoustic model. The a posteriori probability approach computes the a posteriori probability of source location, using the knowledge of the underlying wavefront propagation.

The sound velocity profiles used in this study came from data collected during the 1987 Remote Transmission Experiment in the northern Pacific. A set of twenty four profiles, provided by B. Howe, were taken on a May deployment cruise along a one

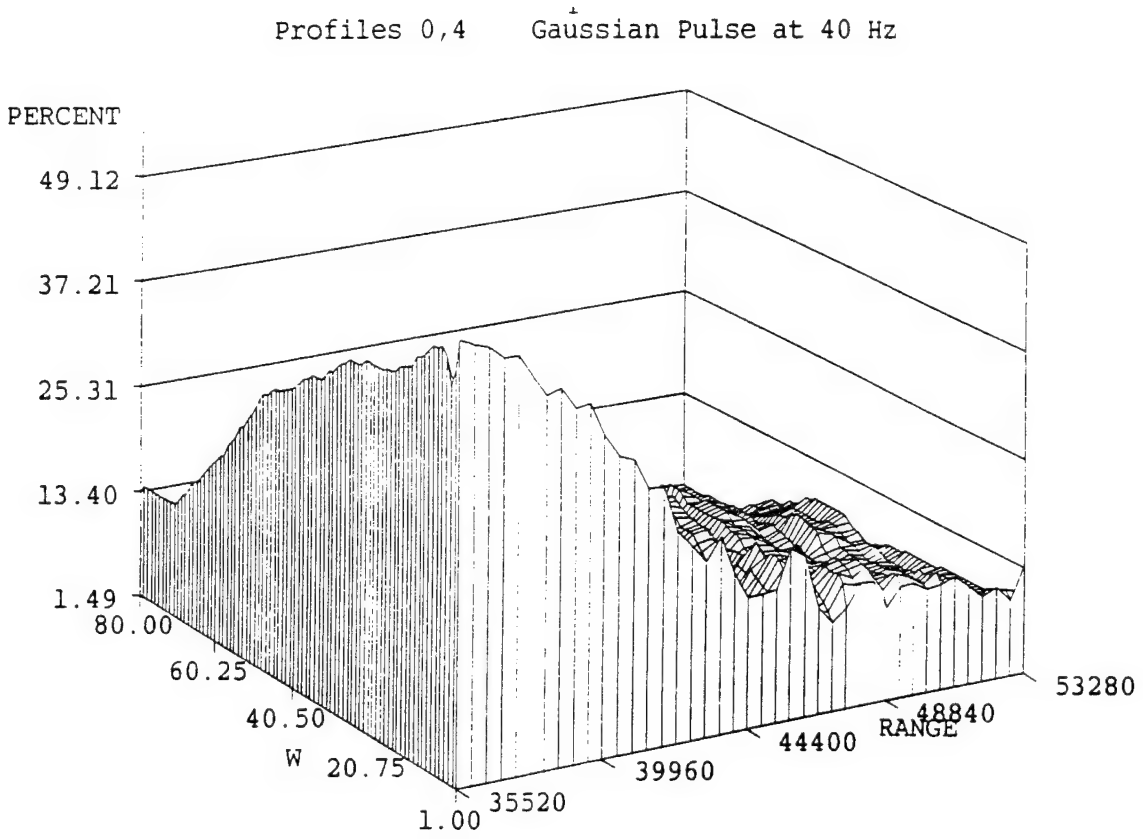

Figure 7: Mismatched performance for profile 4: f = 40 Hz.

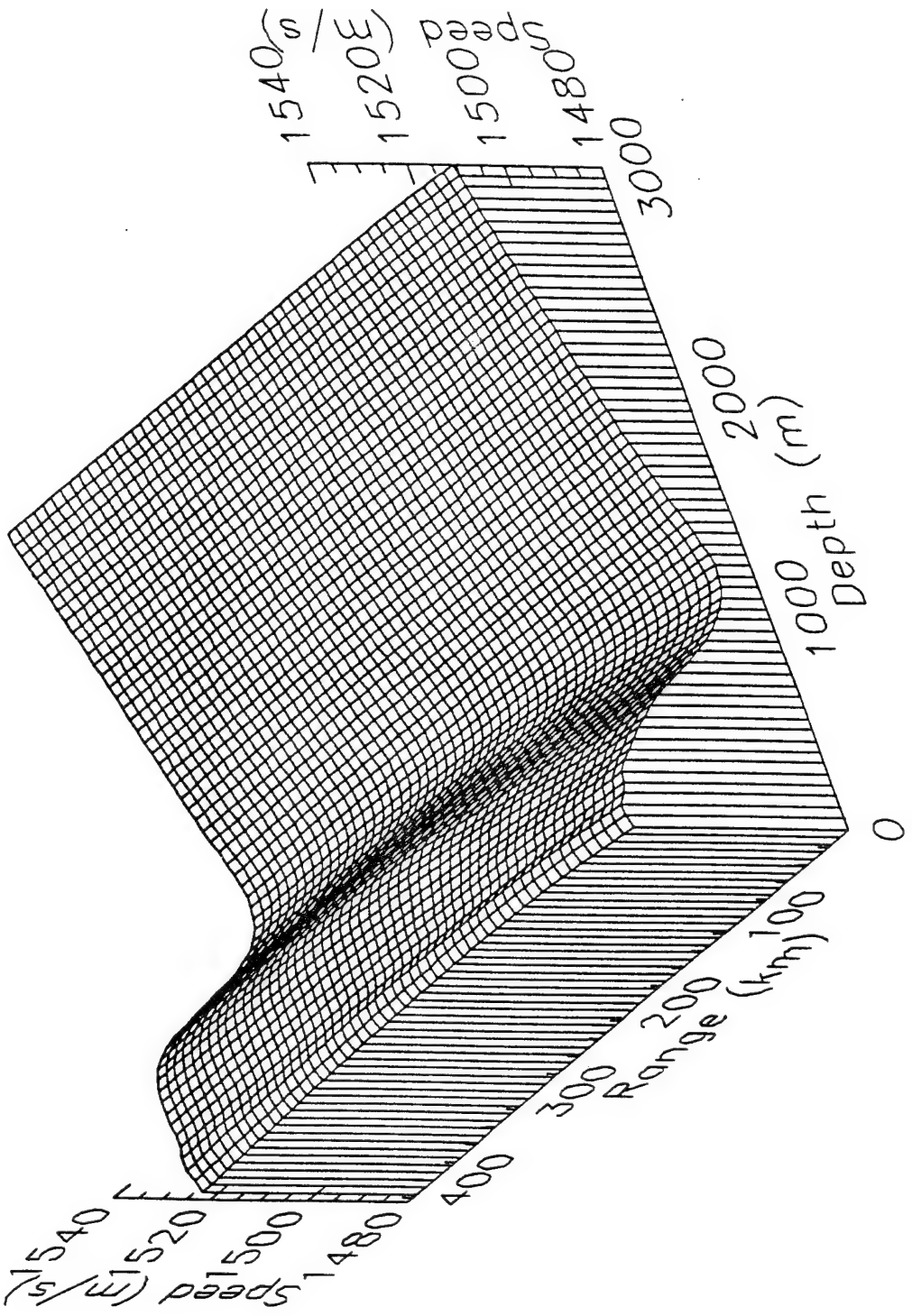

Figure 8: Sound velocity profiles in the gulf stream.

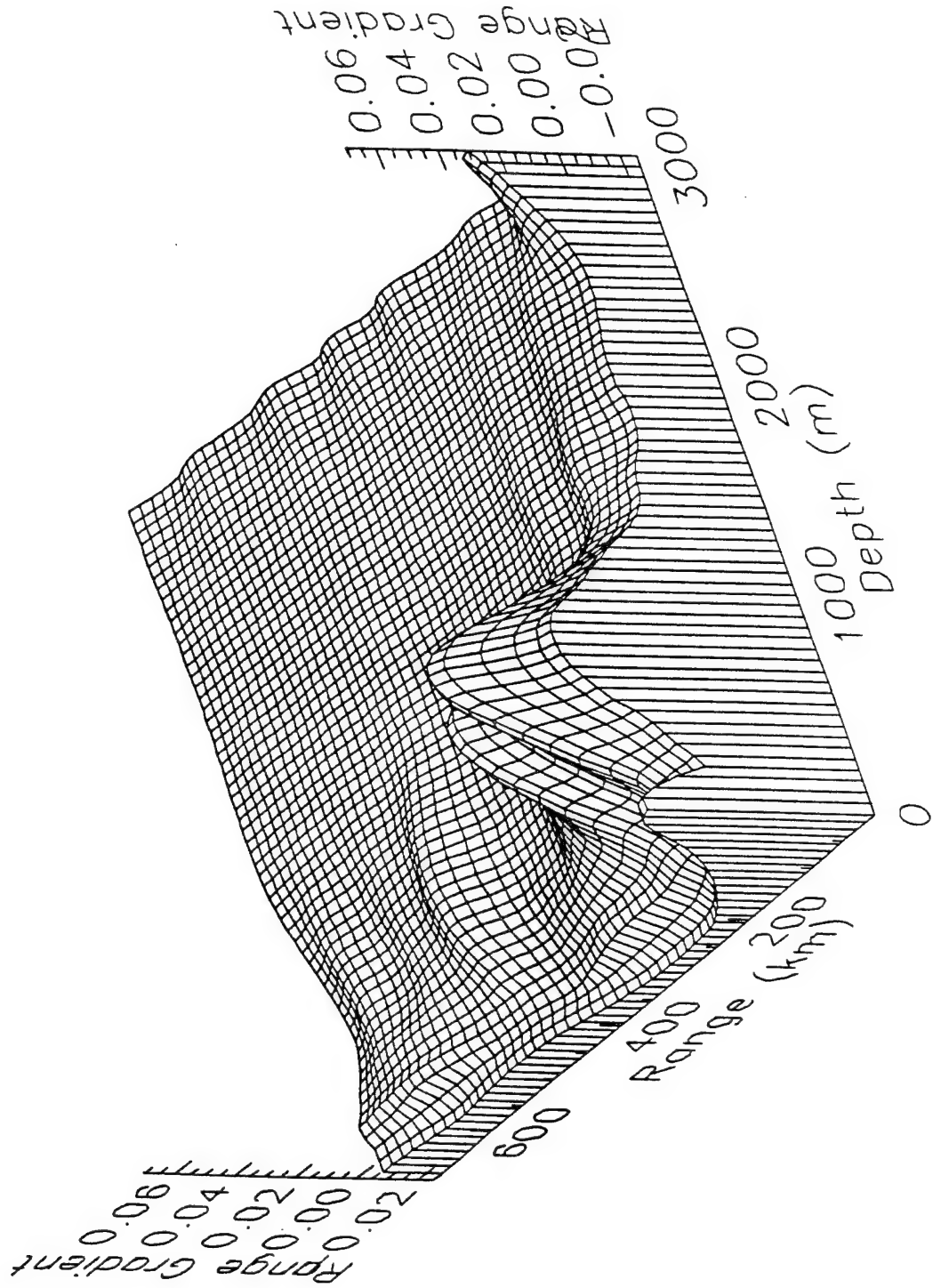

Figure 9: Range gradient; sound velocity profiles in the gulf stream.

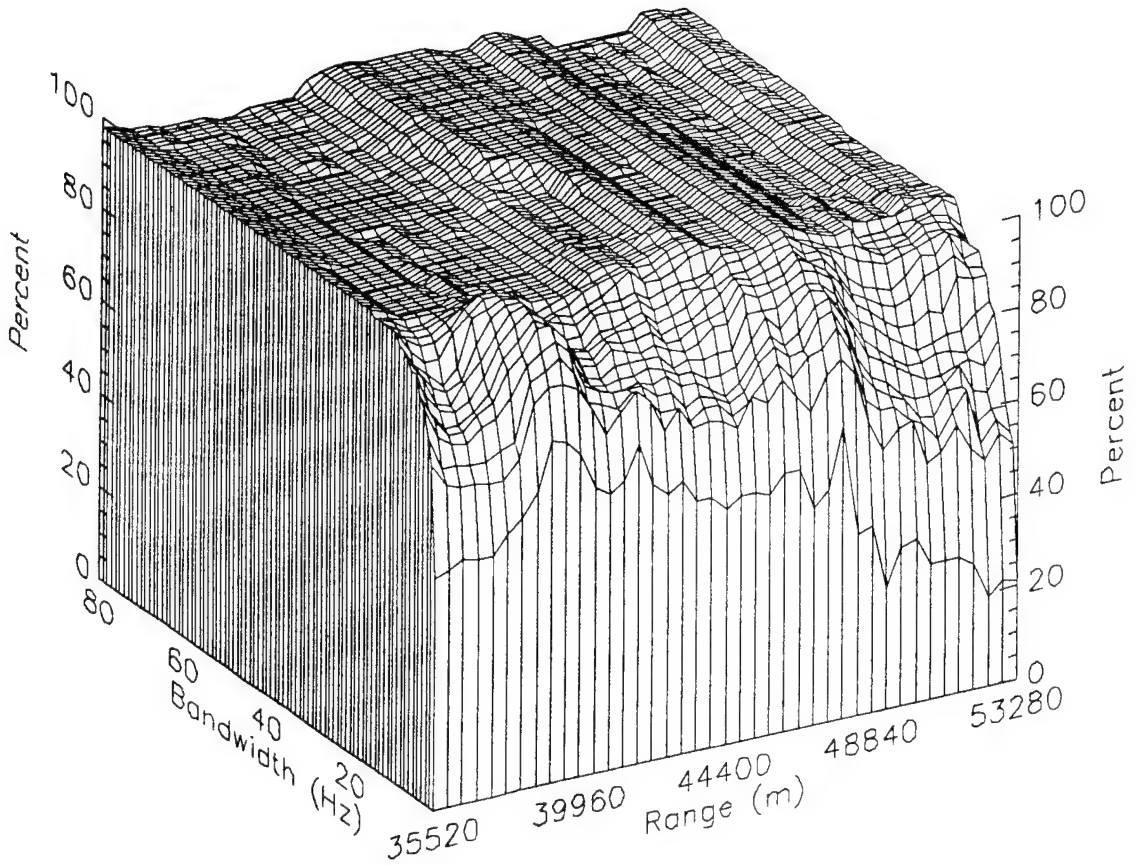

Figure 10: Percentage of points with acceptable performance: f = 40 Hz.

thousand kilometer path. The longitude was a constant 157.1 west. The southern end was at 31.5 north latitude and the northern end was at 40.4 north latitude. The profiles were measured at regular intervals along the path. Another set was taken on the September recovery cruise at approximately the same places. For reference purposes, the 0km/May profile refers to the one taken at the southern end of the path in May. The 1000km/September is the one taken in September at the northernmost point. Range-independent ocean models were made from profiles selected from this varied set. The four profiles used most frequently are shown in Figures 11,12,13,and 14.

In this work the wideband multipath structure of the propagating wavefront, or the space-time impulse response, was exploited for localization. Figure 15 shows impulse responses at five different source ranges with the source at a depth of 1000 meters. Notice that the impulse response shape varies slightly at each of the five different ranges. Figure 16 shows the same effect at the same ranges with the source at a depth of 1500 meters. By comparing the two figures one can see that the impulse response pattern depends on source depth as well as source range. This fact forms the basis of wideband matched field localization. In most of the studies in this section, the amplitudes of the wavefronts were assumed constant and the matching was done only to the arrival time structure.

In the first simulation run, the 0km/May sound speed profile was used. The source is located at a depth of 1000 meters and is 80,800 meters from the receive array. This location was chosen because of the clear multipath effect that takes place at this range. The results are shown in Figure 17. As can be seen from the peak on the plot, the processor localized to within approximately 1000 meters in range and better than 200 meters in depth. However, in the case with the 1000km/May sound speed profile, results are significantly poorer as shown in Figure 18, even though all of the knowledge of the sound speed profile was used here also. This may be explained by the near zero gradient in the upper 300 meters of this profile (Figure 12) and that localization performance inherently varies with the characteristics of the ocean medium.

Matched field processing assumes perfect knowledge of the sound speed profiles. Therefore, cases were run to measure localization performance sensitivity to incorrect profile assumptions. Profiles that differed due to seasonal and geographic changes were used as a test ensemble. In general, depth performance was more resilient than range performance. Mismatching with profiles taken 1000 km apart showed that this was too much variation for good matched field localization in range and depth.

3.3 Optimum Detection and A Posteriori Probability Source Localization

Figures 19 shows optimum detection performance results, on a range-depth receiving grid, for two different bandwidth signals that have propagated through an inhomogeneous ocean channel. Figure 19a shows the evolution of wavefronts, and the resultant multipath

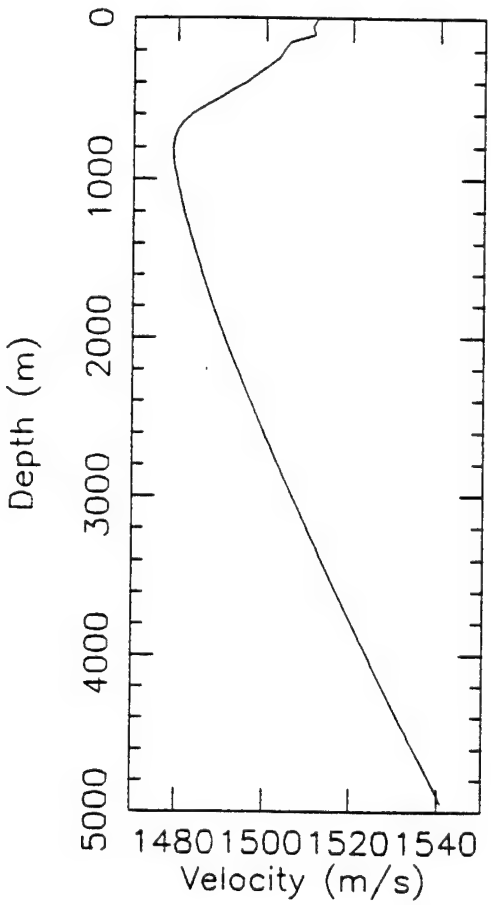

Figure 11: 0km/May sound speed profile.

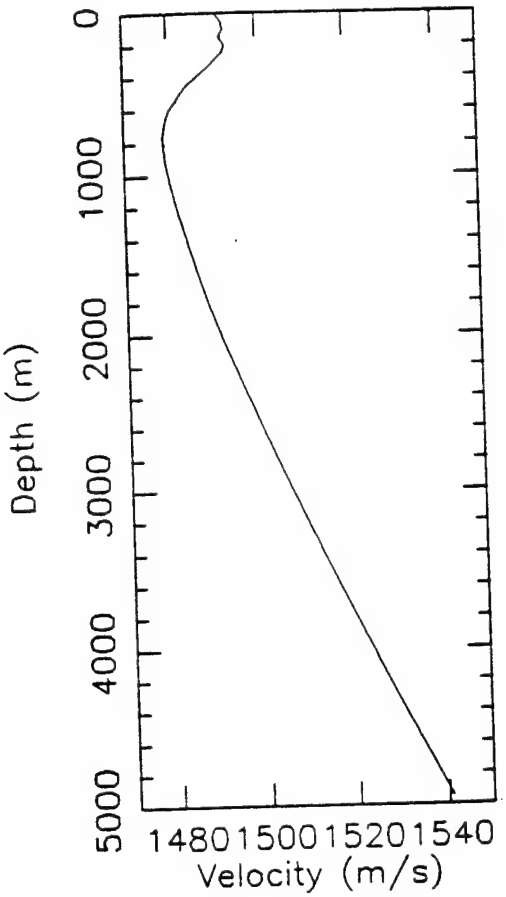

Figure 12: 1000km/May sound speed profile

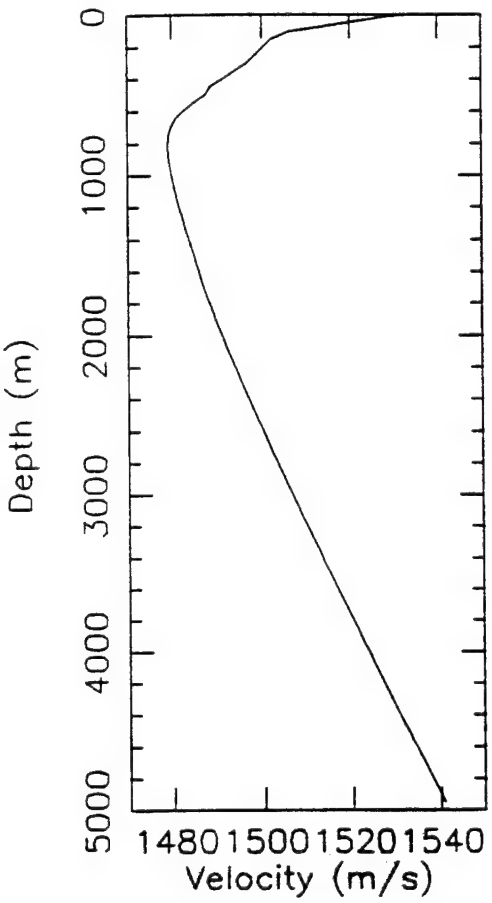

Figure 13: 0km/September sound speed profile

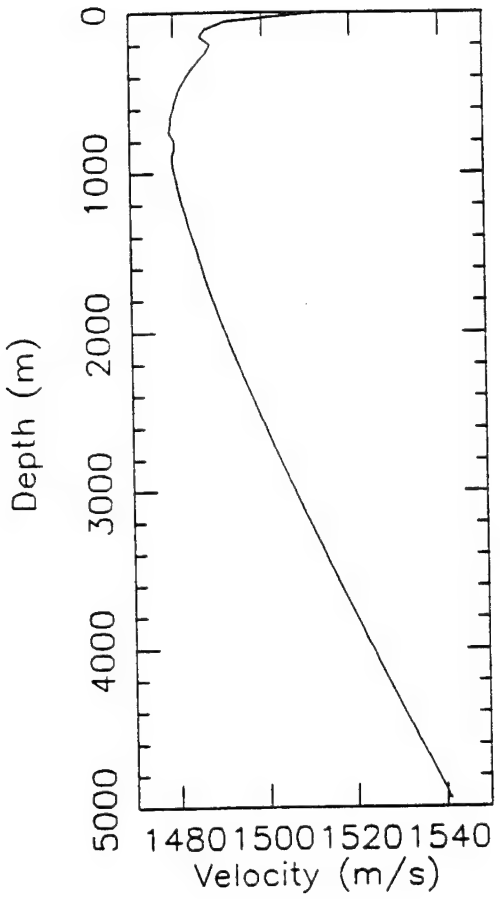

Figure 14: 1000km/September sound speed profile

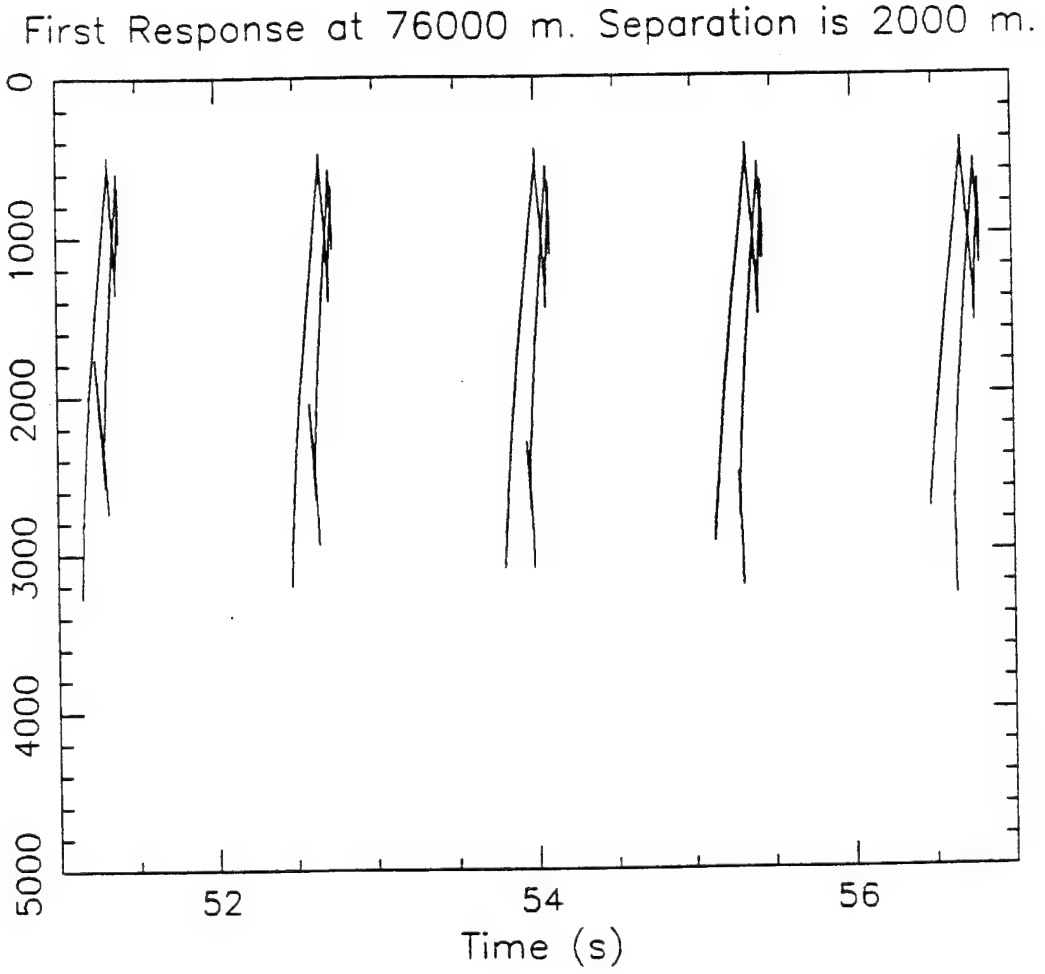

Figure 15: Impulse responses versus range; source depth 1000km

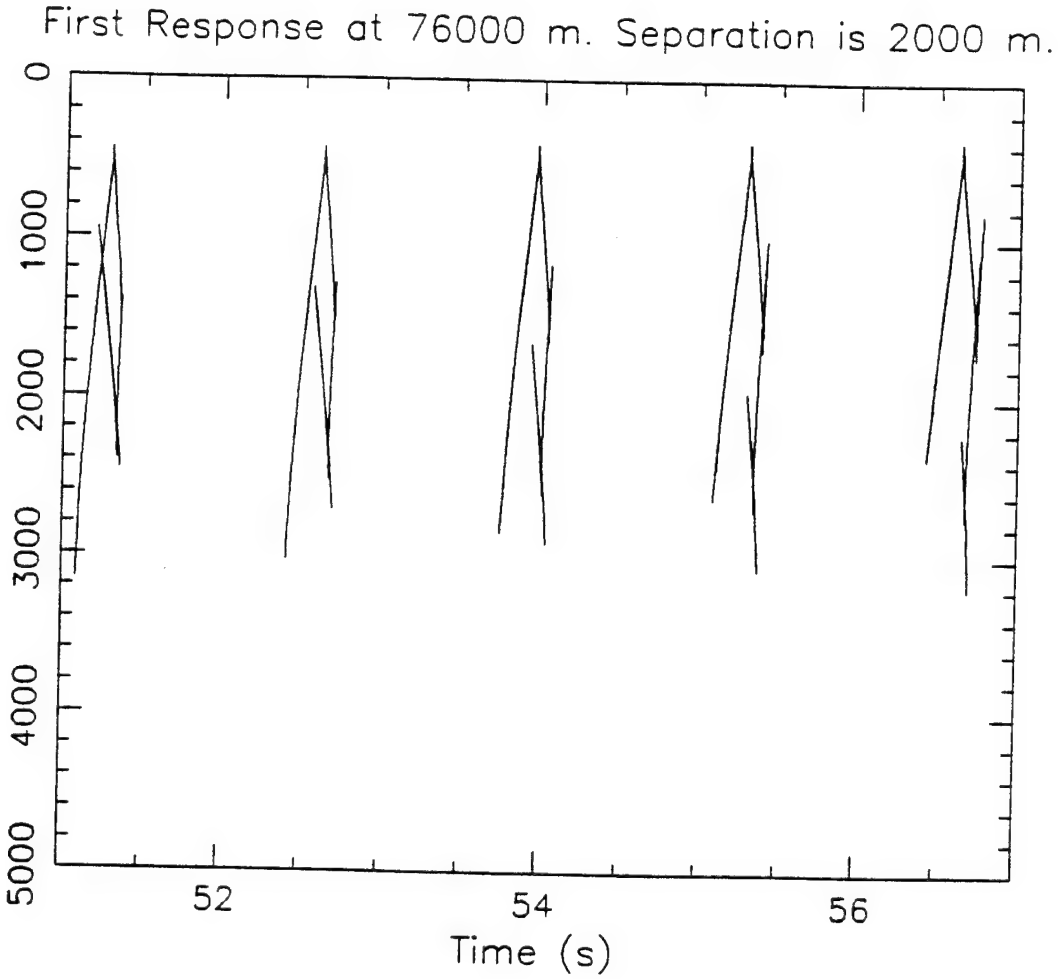

Figure 16: Impulse responses versus range; source depth 1500km

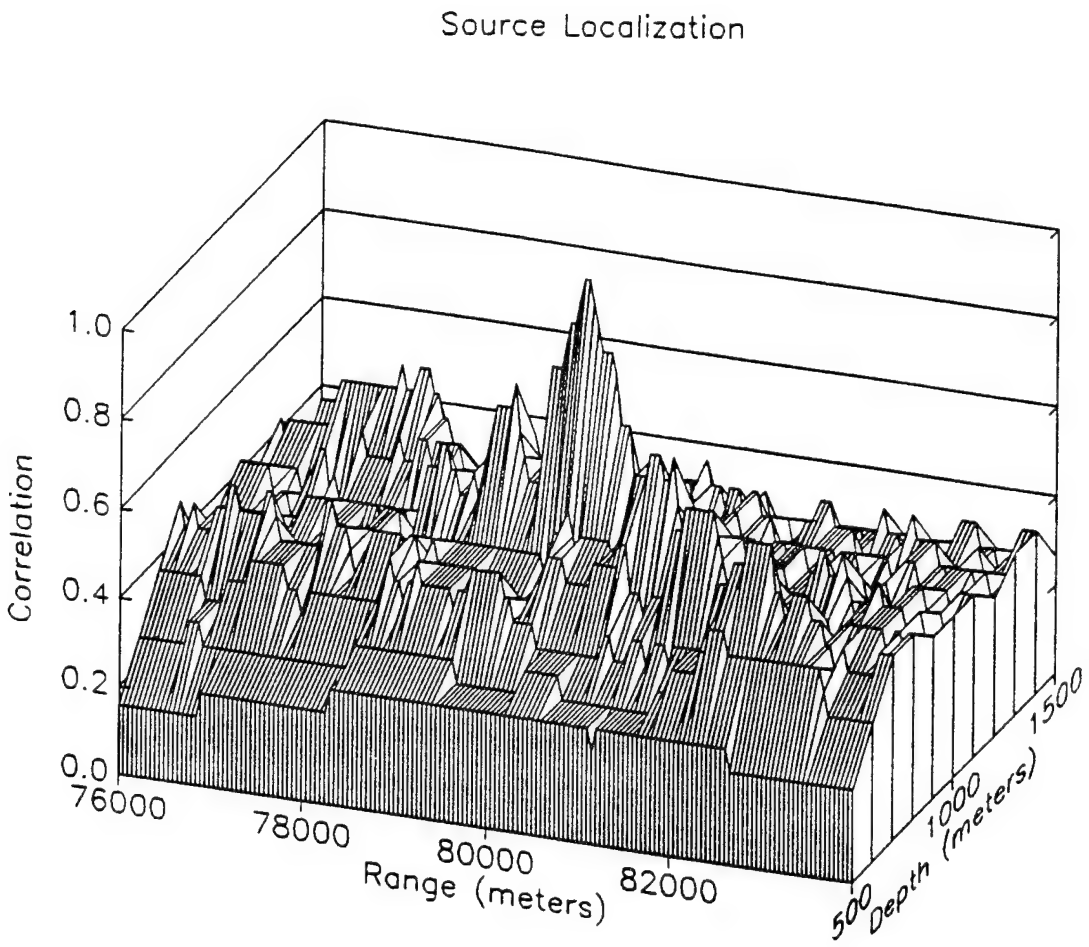

Figure 17: Range-depth localization results with 0km/May Sound Speed Profile

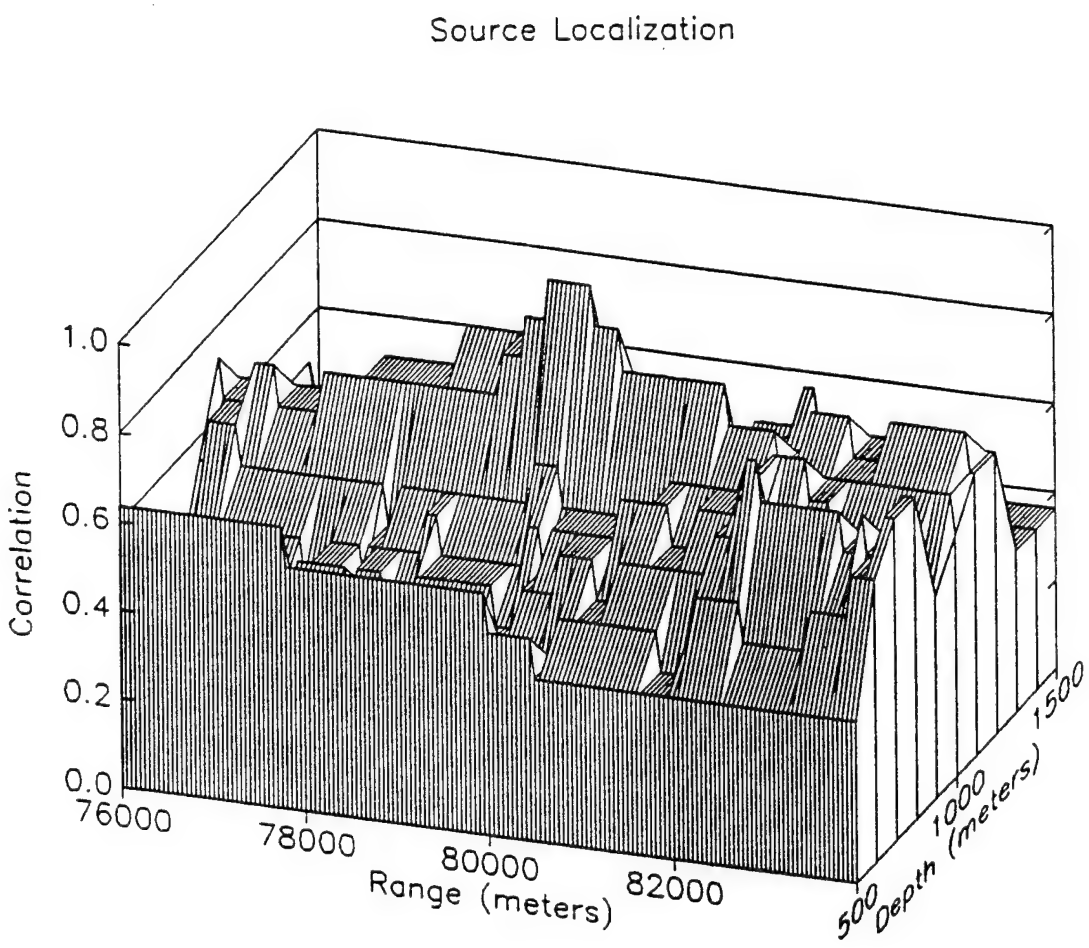

Figure 18: Range-depth localization results with 1000km/May Sound Speed Profile

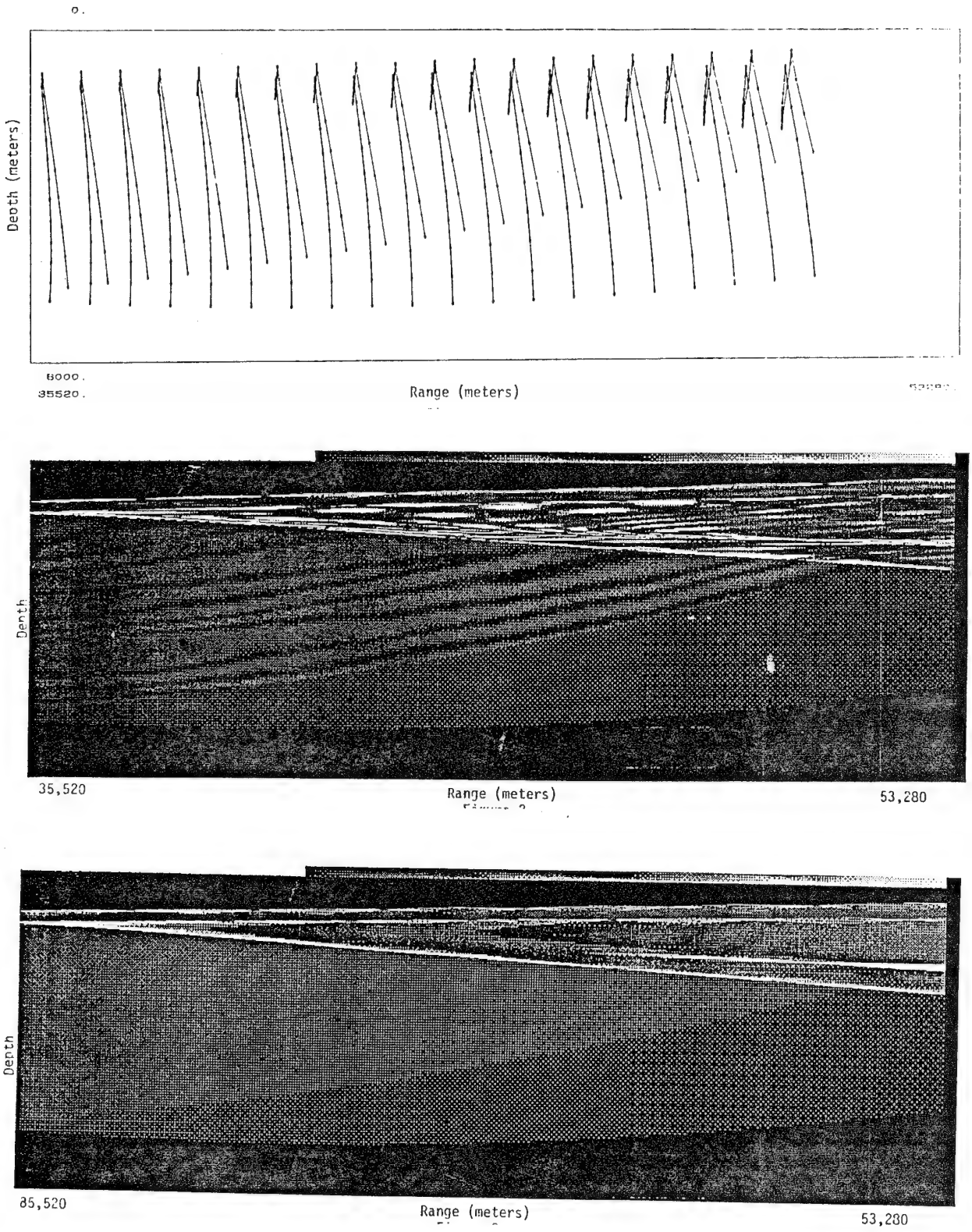

Figure 19: Optimum Detection Performance; Narrowband vs. Wideband

structure, over a range of 35,520 to 53,280 meters at depths to almost 6000 meters. Figure 19b is a plot of amplitudes that are proportional to the detectability index (white corresponds to high values of detectability index) on a grid of 527,030 points over the same range-depth slice, for a narrowband 40 Hz cw signal. A large variability in detection performance is noted, especially in the regions of greater multipath activity. Figure 19c shows the detectability for a 1 Hz bandwidth source signal, where spatial variations in detection performance have been smoothed out considerably.

We have formulated the source localization problem in terms of a range-depth a posteriori probability for long range propagation through an inhomogeneous ocean acoustic medium. Figure 20 illustrates this approach. Figure 20a shows the a posteriori probability for a source with Rayleigh amplitude and uniform phase. Much of the lack of clutter in the a posteriori probability in this case is due to an exponential operation. Figure 20b shows the matched field beamformer output for the same situation.

3.4 Multi-Site Detection Performance

These research results are applicable to the multi-site, widely-spaced arrays, passive ocean surveillance situation. In this work, the design, performance and fault-tolerance of optimum (likelihood ratio) distributed detection networks were investigated [Reibman, Nolte]. This work was begun during the previous research period and completed at the beginning of this report period. The primary effort on this work during this research period was the preparation of the papers [Reibman, Nolte]. Detailed research results are available in these published papers.

In this framework only local decisions, rather than all of the data, are transmitted from distant sites to a central processing facility. An advantage of this approach is the narrower communications bandwidths required. However, this advantage comes at the cost of reduced detection performance. The loss in detection performance was determined over that which would have been attained had all of the data been transmitted back to the central processing facility from the distant multi-sites.

The optimal design of each local processor in the distributed network is shown to be the likelihood ratio. The local thresholds are computed from coupled equations, related by functions of the local processor false alarm and detection probabilities. Network performance is also expressed using local processor performance. Hence, the optimal network performance may be computed knowing only the local performance. The signal and noise statistics that underly the local performance is not essential.

A series of studies on the performance of distributed detection networks were made. The first study examined the performance improvement available when the optimal design for a given network is used. Intuitive choices of the optimal fusion design are shown to yield suboptimal performance.

The remainder of the studies examine the tradeoff of network structure on the performance of optimally designed systems. The performance of serial and fusion networks are

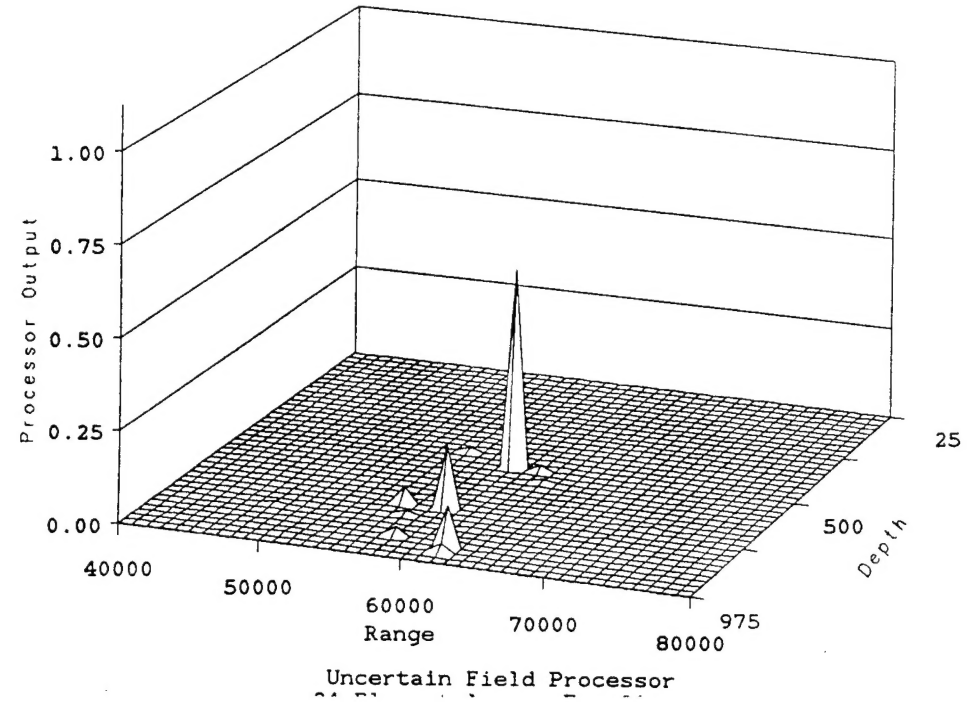

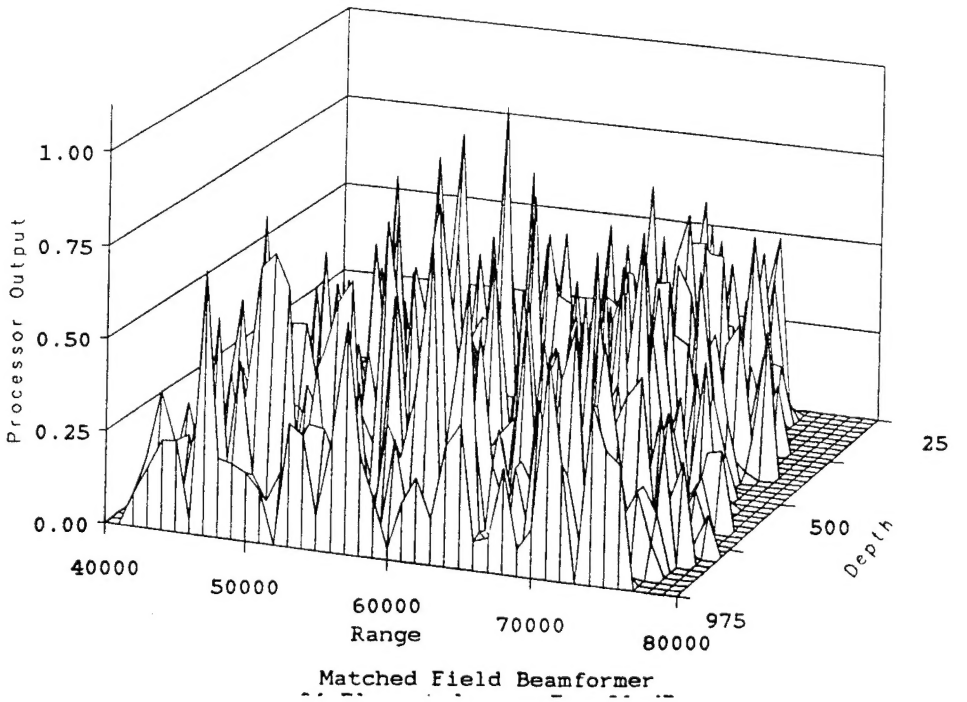

Figure 20: Localization; a posteriori probability versus matched field

compared both for small and large networks. For small networks, the serial network has better performance than the fusion network. However, for large numbers of local processors, the fusion network has better performance. The number of processors necessary before the fusion network becomes better depends on the noise environment.

The performance of the networks was also examined when processor faults may occur. The optimal fault-tolerant design is obtained, both for the distributed networks and the centralized system. The performance improvement of the fault-tolerant system is presented. Also, the effect of the number of processors and fault probability on fault-tolerant performance is examined. Finally, the fault-tolerant fusion network is shown to have better performance that a faulty central processor for many observation vectors.

4 Participating Scientific Personnel

- Karen Frenzel, "Detection of a Random Signal in a Multi-Channel Environment: A Performance Study," Ph.D. Thesis, Duke University, 1986.
- Richard A. Marshall, "Detection of Known Signals in Spatially Correlated Noise," M.S.E. Thesis, Duke University, 1986.
- Amy R. Reibman, "Performance and Fault-Tolerance of Distributed Detection Networks," Ph.D. Thesis, Duke University, 1987.
- Howard A. Lazoff, "Underwater Detection Performance and Sensitivity to Sound Velocity Profile Variations," M.S.E. Thesis, Duke University, 1988.
- Nancy Rausch, "Ocean Acoustic Source Localization," M.S.E. Thesis, Duke University, 1989.
- Robert Clarke III, "Range-Depth and Range Angle Localization of an Ocean Acoustic Source," M.S.E. Thesis, Duke University, 1989.
- Anthony M. Richardson, Ph.D. student

5 Publications and Papers

- L. W . Nolte, S. C. Lee and S. C. Liu (invited paper), "On Performance of Array Signal Processing," *IEEE Journal of Oceanic Engineering* , Vol. OE-12, No. 1, pp. 148-154, January 1987
- A. M. Richardson, and L. W. Nolte, "Underwater Acoustic Multipath Signal Processing," *19th Southeastern Symposium on System Theory*, Clemson, South Carolina, March 1987.
- A. Reibman and L. W. Nolte, "Optimal Detection and Performance of Distributed Sensor Systems", *IEEE Transactions on Aerospace and Electronic Systems*, Vol. AES-23, No. 1, January 1987, pp. 24-30.
- A. Reibman and L. W. Nolte, "Performance of Distributed Detection Systems", in *Proceedings 19th Southeastern Symposium on System Theory*, pp. 236–239, Clemson, S. C., March 1987.
- L. W. Nolte and A. M. Richardson, (invited paper), "On Optimum Sound-Velocity-Profile Based Signal Detection," *Twenty-first Annual Asilomar Conference on Signals, Systems, and Computers*, Pacific Grove, CA, November 1987.

- A. Reibman and L. W. Nolte, "Design and Performance Comparison of Distributed Detection Networks", *IEEE Transactions on Aerospace and Electronic Systems*, Vol. AES-23, No. 6, pp. 789-797, November 1987.
- A. Reibman and L. W. Nolte, "Detection Performance of Two-sensor Distributed Systems for Normal Local ROCs", *Proceedings 26th IEEE Conference on Decision and Control*, pp. 1616–1617, Los Angeles, CA, December 1987.
- A. Reibman and L. W. Nolte, "Performance of Redundant and Distributed Detection Systems with Processor Faults", *Proceedings 1988 IEEE International Conference on Acoustics, Speech, and Signal Processing*, New York, N. Y., April 1988.
- L. W. Nolte and A. Reibman, (invited paper), "On Determining the Design for Fusion Detection Networks", *27th IEEE Conference on Decision and Control*, December 1988.
- A. Reibman and L. W. Nolte, "Optimal Fault-tolerant Signal Detection," *IEEE Transactions on Acoustics, Speech, and Signal Processing*, Vol. 38, Issue 1, pp. 179-181, January 1990.
- A. Richardson and L. W. Nolte, "Performance and Sensitivity of Matched Field and Uncertain Field Processor Approaches", *Meeting of the Acoustical Society*, State College, Pennsylvania, May 1990.